Reopening the Z portal with semi-annihilations

María J. Domínguez,[1,*] Oscar Rodríguez,[1,2,†] and Óscar Zapata[1,‡]

[1]*Instituto de Física, Universidad de Antioquia, Calle 70 # 52-21, A.A. 1226 Medellín, Colombia*
[2]*Facultad de Ingenierías, Universidad de San Buenaventura, Carrera 56C # 51-110, Medellín, Colombia*

(Received 12 June 2024; accepted 6 August 2024; published 29 August 2024)

In one-component dark matter (DM) scenarios is commonly assumed that a scalar weakly interacting massive particle must either be part of an $SU(2)_L$ multiplet with zero hypercharge or have suppressed vector interactions with the Z-gauge boson to circumvent stringent direct detection (DD) bounds. In this work, we demonstrate that multicomponent scenarios with a dark scalar doublet exhibiting vectorlike interactions with the Z boson are also compatible with bounds arising from DD searches. Specifically, we consider a simple extension of the Standard Model wherein the dark sector comprises a doublet and a complex singlet ϕ, both charged under a Z_6 symmetry. We find that semi-annihilation processes drastically reduce the relic abundance of the neutral component of the doublet, H^0, sufficiently attenuating the effects of its large Z-mediated elastic scattering cross-section with nucleons to satisfy the DD constraints. Although the contribution of H^0 to the total relic abundance is nearly negligible, with ϕ dominating, both dark matter components are expected to be detectable in ongoing and future DD experiments. The viability of the model is tested against several theoretical and experimental constraints, resulting in a parameter space featuring a nondegenerate mass spectrum at the electroweak scale.

DOI: 10.1103/PhysRevD.110.035034

I. INTRODUCTION

The observed relic abundance of dark matter (DM) [1] finds a simple and appealing explanation through a new stable particle characterized by electroweak-scale mass and interactions [2]. This particle achieves chemical equilibrium with the Standard Model (SM) in the early Universe, following the weakly interacting massive particle (WIMP) mechanism [3,4]. In this context, the SM Higgs and Z bosons may act as mediators between the dark and visible sectors, giving rise to the Higgs-portal [5,6] and Z-portal [7] models. Among the simplest models accommodating the Higgs portal are those that introduce a SM singlet, either a scalar [8–10] or a fermion [11–13]. Conversely, the archetype of a purely Z-mediated DM model is the neutralino [3,14]. Notably, renormalizable DM models encompassing both Higgs and Z portals, such as the inert doublet model (IDM) [15,16], can be easily found.

Direct searches [17] have been crucial in probing large portions of the parameter space of WIMP models. Indeed, in models having an open Z-portal they exclude DM candidates that can elastically scatter on nuclei via a tree-level Z-boson exchange due to a spin-independent (SI) cross section lying orders of magnitude above the current bounds [18–20]. This situation materializes, for instance, in the IDM where the neutral component of the inert doublet acts as the DM candidate, leading to a large scattering cross section with nuclei of the order of 10^{-39} cm^2 [16]. Nonetheless, it is only when the CP components of the doublet are nondegenerate (leading to a nondiagonal coupling to Z boson) that the stringent direct detection (DD) limits can be circumvented. This enables the explanation of the observed DM abundance for masses near the Higgs resonance and exceeding 500 GeV [21].

DM in the Universe may not necessarily made up of a single particle and instead populated by several species accounting for the total abundance [22–29]. In these frameworks, new DM processes [30,31] such as conversions and semi-annihilations typically arise, modifying not only the production of each component but also their interactions with the visible sector, thus providing a reason for the lack of DD signatures in single DM component scenarios. Certainly, recent phenomenological studies on multicomponent WIMP models (see e.g., Refs. [32–58]) have shown that their compatibility with current experimental data is possible even with DM masses significantly less than 1 TeV.

In this work, we analyze a two-component DM model with two scalar candidates; a SM singlet ϕ and the neutral

*Contact author: mjose.dominguez@udea.edu.co
†Contact author: oscara.rodriguez@udea.edu.co
‡Contact author: oalberto.zapata@udea.edu.co

component H^0 of a second weak-isospin doublet H_2, both charged under a Z_6 symmetry.[1] Both candidates retain their complex nature even after electroweak (EW) symmetry breaking, implying that H^0 continues having diagonal gauge interactions with the Z boson. We demonstrate that the semi-annihilation processes induced by the interaction term $H_2^\dagger H_1 \phi^2$ cause a large suppression on the H^0 abundance in such a way the expected number of events associated with H^0 in DD experiments, such as LUX-ZEPLIN (LZ) [19], can lie below the current upper bound. Moreover, this conclusion is obtained guaranteeing that all constraints imposed on the model are fulfilled in a range of nondegenerate DM masses around the EW scale. In this way, the doublet candidate not only emerges as a valid candidate but also can leave signatures in current and future DM experiments.

The rest of the paper is organized as follows. In the next section, we present the model and study the effect of the interactions allowed by the Z_6 symmetry on the DM relic densities, as well as the DD of the DM candidates. Special emphasis is placed on calculating the expected number of events in xenon-based experiments. In Sec. III, we describe the theoretical and experimental constraints that must be satisfied and determine the viable parameter space through random scans. This analysis also includes an investigation of detection prospects. Finally, we present our conclusions in Sec. IV.

II. THE MODEL

The model we consider enlarges the SM by introducing a dark scalar sector made up of a second Higgs doublet H_2 and a complex gauge singlet ϕ. Besides, an exact Z_6 symmetry is introduced such that the dark sector fields are charged under Z_6 whereas the SM fields transform trivially. In order to have two DM candidates, besides imposing that the new scalar fields do not acquire a nonzero vacuum expectation value, the neutral component of H_2 and ϕ must not mix with each other.[2] The charge assignment assuring these conditions becomes[3]

$$Z_6(\phi) = \omega_6, \qquad Z_6(H_2) = \omega_6^2, \qquad \omega_6 = e^{i\pi/3}. \tag{1}$$

Consequently, the most general Z_6-invariant scalar potential reads,

$$\begin{aligned}\mathcal{V} = &-\mu_1^2|H_1|^2 + \lambda_1|H_1|^4 + \mu_2^2|H_2|^2 + \lambda_2|H_2|^4 + \mu_\phi^2|\phi|^2 \\ &+ \lambda_\phi|\phi|^4 + \lambda_3|H_1|^2|H_2|^2 + \lambda_4|H_1^\dagger H_2|^2 + \lambda_6|H_2|^2|\phi|^2 \\ &+ \frac{1}{2}\lambda_7\left(H_2^\dagger H_1 \phi^2 + \text{H.c.}\right) + \lambda_8|H_1|^2|\phi|^2,\end{aligned} \tag{2}$$

where H_1 represents the SM Higgs doublet and λ_7 is real without loss of generality, achievable through field redefinitions of ϕ, H_1, or H_2. Working in the unitary gauge,

$$H_1 = \begin{bmatrix} 0 \\ \frac{1}{\sqrt{2}}(v+h) \end{bmatrix}, \qquad H_2 = \begin{pmatrix} H^+ \\ H^0 \end{pmatrix}, \tag{3}$$

with $v = 246$ GeV, the scalar spectrum is given by

$$m_h^2 = 2\lambda_1 v^2, \tag{4}$$

$$m_\phi^2 = \mu_\phi^2 + \frac{v^2}{2}\lambda_8, \tag{5}$$

$$m_{H^\pm}^2 = \mu_2^2 + \frac{v^2}{2}\lambda_3, \tag{6}$$

$$m_{H^0}^2 = \mu_2^2 + v^2\lambda_L, \tag{7}$$

with $\lambda_L \equiv (\lambda_3 + \lambda_4)/2$. When ϕ is the lightest particle we impose the kinematic relation $m_{H^0} < 2m_\phi$ to ensure the stability of H^0. Notice that the absence of the term $[\lambda_5(H_1^\dagger H_2)^2 + \text{H.c.}]$ entails that the H^0 field remains complex, i.e., the CP-even and CP-odd components have the same mass. Fixing the Higgs boson mass m_h at 125 GeV [65], the model includes nine new free parameters; six dimensionless $(\lambda_2, \lambda_3, \lambda_6, \lambda_8, \lambda_\phi, \lambda_L)$ and three dimensionful chosen to be the dark scalar masses.

The set of new scalar interactions induces annihilation, semi-annihilation and conversion processes which affect DM relic densities in distinctive ways. First, the usual Higgs portal interactions, (λ_3, λ_4) for the doublet and λ_8 for the singlet, couple the DM particles with the SM ones, leading to DM self-annihilation processes (see Fig. 1). Secondly, as is shown in Fig. 1, DM conversion processes can arise in three different ways; from the quartic terms λ_6 and λ_7, and from the interplay of the two Higgs portal interaction terms. Thirdly, the Higgs portal interactions also play a role in the semi-annihilation processes when combined with the λ_7 interaction, although such processes appear independently of the Higgs portal (see Fig. 2).[4] Finally, the self-interacting terms, λ_ϕ and λ_2, although not relevant for the DM phenomenology, they play a key role in ensuring the theoretical consistency of the model.

[1] For scenarios involving a Z_6 symmetry responsible for DM stability, see Refs. [53,59–61].

[2] Notice that the model presented in Ref. [42] considers the neutral components of H^0 to be nondegenerate.

[3] The discrete symmetry can be promoted to a $U(1)_X$ global symmetry, leading to the charge assignment $X(H_2) = 2X(\phi)$ and $X(\text{SM}) = 0$, such that $2X(\phi) - X(H_2) = 0$. Recall that this possibility opens the door to considering a dark asymmetry [62] within a two-component scenario [63,64].

[4] See Ref. [66] for a study of semi-annihilations in models including one or two scalar multiplets in the dark sector.

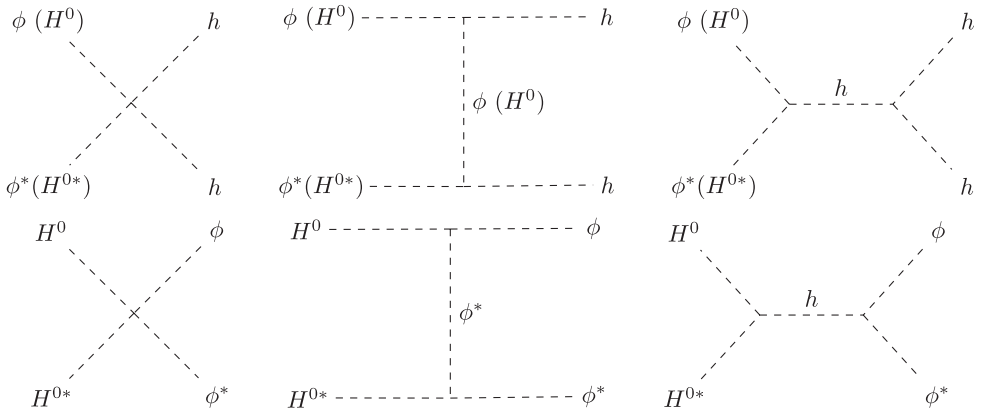

FIG. 1. Top: DM self-annihilation processes mediated by the Higgs portal interactions. Final states as WW, ZZ, hZ, and $f\bar{f}$ can be also present in the s-channel processes. Bottom: DM conversion processes mediated by the λ_6 (left panel), λ_7 (middle panel), and the Higgs portal (right panel) interactions.

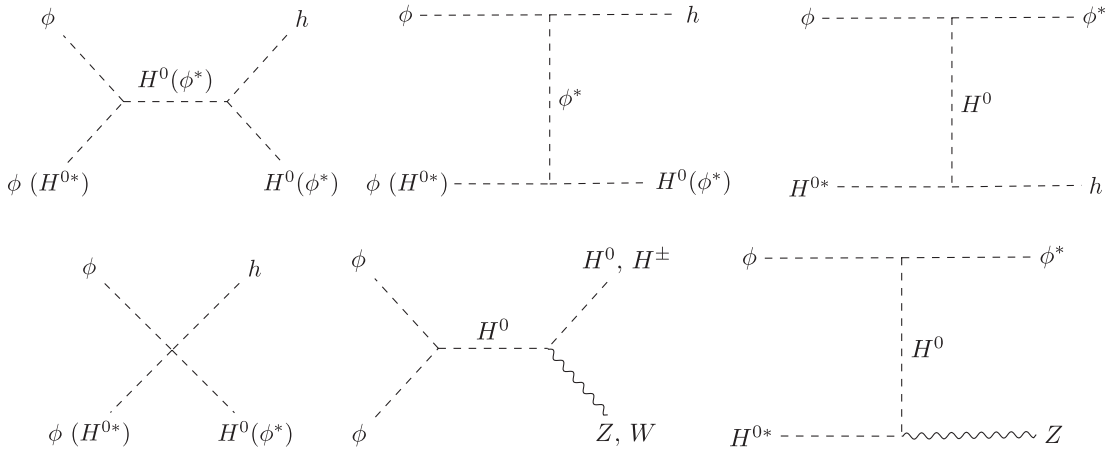

FIG. 2. DM semi-annihilation processes mediated by the interplay of Higgs portal and λ_7 interactions (top panels), by only the λ_7 interaction (bottom left panel) and by the interplay between the λ_7 and the gauge portal interactions (bottom middle and right panels).

On the other hand, gauge interactions of the doublet H_2 not only cause (co)annihilation processes but also semi-annihilation processes. The first set involves new processes such as $H^0H^0 \to WW$ but also as those mediated by the Higgs portal $H^0H^0 \to hh$, among others. The second set brings with the purely new type of processes involving a gauge boson in the final state thanks to the presence of the λ_7 interaction term, as displayed in the bottom panels (center and right) of Fig. 2. As will be shown in the next section, this type of processes is fundamental to evade the DD constraints.

Table I summarizes all the $2 \to 2$ processes that may affect the relic densities of ϕ and H^0. These processes are classified according to the fields involved and to the number of SM particles present in the final state. To this end, ϕ/ϕ^* and H_2/H_2^* are assumed to belong, respectively, to sectors 1 and 2, whereas the SM particles belong to

TABLE I. The $2 \to 2$ processes allowed (at tree level) by the Z_6 symmetry and that can modify the relic density of ϕ (top) and H^0 (bottom). Z and $W^\pm$ denote the EW gauge bosons whereas h stands for the SM Higgs boson. Conjugate and inverse processes are not shown.

ϕ processes	Type
$\phi + \phi^* \to SM + SM$	1100
$\phi + \phi^* \to H^0 + H^{0*}$	1122
$\phi + \phi \to H^0 + h(Z), H^\pm + W^\mp$	1120
H^0 processes	Type
$H^0 + H^{0*} \to SM + SM$	2200
$H^0 + H^{0*} \to \phi + \phi^*$	2211
$H^0 + h \to \phi + \phi$	2011
$H^{0*} + \phi \to \phi^* + h(Z)$	1210

sector 0. In this way, processes of the type 1100, 2200, and 1200 correspond to (co)annihilations, whereas 1110, 2220, 1120, 2210, 1210, and 1220 denote semi-annihilation processes. DM conversion processes are of the type 1122 and 2211.

A. Relic abundance

The Boltzmann equations for the model can then be written down as

$$\frac{dn_\phi}{dt} = -\sigma_v^{1100}(n_\phi^2 - \bar{n}_\phi^2) - \sigma_v^{1120}\left(n_\phi^2 - n_{H^0}\frac{\bar{n}_\phi^2}{\bar{n}_{H^0}}\right) - \sigma_v^{1122}\left(n_\phi^2 - n_{H^0}^2\frac{\bar{n}_\phi^2}{\bar{n}_{H^0}^2}\right) - 3Hn_\phi, \tag{8}$$

$$\frac{dn_{H^0}}{dt} = -\sigma_v^{2200}(n_{H^0}^2 - \bar{n}_{H^0}^2) - \sigma_v^{2211}\left(n_{H^0}^2 - n_\phi\frac{\bar{n}_{H^0}^2}{\bar{n}_\phi^2}\right) - \frac{1}{2}\sigma_v^{1210}\left(n_\phi n_{H^0} - n_\phi \bar{n}_{H^0}\right) - \sigma_v^{1120}\left(n_\phi^2 - n_{H^0}\frac{\bar{n}_\phi^2}{\bar{n}_{H^0}}\right) - 3Hn_{H^0}, \tag{9}$$

where σ_v^{abcd} stands for the thermally averaged cross section, which satisfies $\bar{n}_a\bar{n}_b\sigma_v^{abcd} = \bar{n}_c\bar{n}_d\sigma_v^{cdab}$, H is the Hubble constant, n_ψ denotes the number density of the ψ field and $\bar{n}_\psi$ its the respective equilibrium value. To numerically solve these equations and obtain the relic densities of ϕ and H^0 (denoted here as Ω_ϕ and Ω_{H^0}, respectively), we used micrOMEGAs [67,68] (via LanHEP [69]) which automatically takes into account all the relevant processes for a given model.

We begin our analysis by considering a set of reference models to understand how the new conversion and semi-annihilation processes modify the DM abundances during freeze-out. In what follows, we fix the λ_8 and λ_L scalar couplings to 0.1 and $m_{H^\pm}/m_{H^0} = 1.1$. Two mass hierarchies are considered; $m_\phi < m_{H^0} < m_{H^\pm}$ and $m_{H^0} < m_{H^\pm} < m_\phi$. To observe the effect on Ω_ϕ and Ω_{H^0} due to the DM conversion induced by λ_6, we take $\lambda_7 = 0$. On the other hand, fixing $\lambda_6 = 0$ but keeping $\lambda_7 \neq 0$, we are able to appreciate the effect of the DM semi-annihilation processes.

We first analyze the absence of semi-annihilations ($\lambda_7 = 0$) for the two mass hierarchies and different values of λ_6 when the DM mass ratio is fixed at 1.2 (see Fig. 3). In particular, we allow λ_6 to vary as 0.0, 1.0, 3.0. In the scenario where ϕ is the lightest DM component (top panels), the λ_6 interaction significantly affects the value of Ω_{H^0} (up to two orders of magnitude for intermediate values of m_{H^0}), while the effect on Ω_ϕ is negligible. Ω_ϕ is then determined by the same Higgs-mediated interactions of the scalar singlet model, resembling the singlet scalar DM model. When the doublet component is the lightest one (bottom panels), λ_6 deeply affects Ω_ϕ, with a variation of approximately three orders of magnitude over the mass range considered for ϕ. The effect on Ω_{H^0} is, on the contrary, slightly small. In this case, Ω_{H^0} is basically determined by the Higgs and gauge portal interactions as occurs in the IDM.

Next, we take $\lambda_6 = 0$ and consider the effect of the DM semi-annihilation processes when λ_7 is varied as 0.1, 1.0, 3.0. From Fig. 4, it can be observed that when ϕ is the lightest DM component, Ω_{H^0} decreases with λ_7 in several orders of magnitude over a mass range which widens with the value of mass ratio m_{H^0}/m_ϕ. In the top panels, this ratio is fixed at 1.2, whereas a value of 1.6 is chosen for the bottom panels. This behavior is a consequence of the exponential suppression

$$\frac{dn_{H^0}}{dt} \propto \sigma_v^{1210} n_\phi n_{H^0}, \tag{10}$$

present in the Boltzmann equation [Eq. (9)] and associated with the semi-annihilation processes $\phi + H^{0*} \leftrightarrow \phi + h$ and $\phi + H^{0*} \leftrightarrow \phi + Z$ (see Fig. 2), which do not modify the singlet abundance. This is because in the low-mass region the semi-annihilation processes that alter the number density of ϕ are kinetically suppressed, so that Ω_ϕ is governed mainly by the usual Higgs interactions. When the $\phi + \phi \to H^{0*} + h(Z)$ channels are open, Ω_{H^0} grows rapidly at the expense of a decrease of Ω_ϕ of up to three orders of magnitude at the intermediate mass scale. Now, if H^0 turns out to be the lightest DM component, the impact of the λ_7 interaction on Ω_{H^0} is small, that is, instead of a large reduction like that shown in Fig. 4, only a variation of at most one order of magnitude takes place for the different values of λ_7 on the range of m_{H^0} (see Fig. 5). Nevertheless, the DM semi-annihilation processes induced by λ_7 do significantly affect Ω_ϕ, although their impact is largely independent of m_ϕ/m_{H^0}.

As will be discussed in the next section, a suppression of at least six orders of magnitude on Ω_{H^0} is necessary for evading the exclusion limits on the H^0 SI cross section. In accordance with the discussion so far, this is possible only for a mass regime in which $m_{H^0} > m_\phi$. Therefore, hereafter we focus our analysis on the scenario where ϕ is the lightest DM component.[5] As a comment aside, we stress that the exponential suppression on Ω_{H^0} in the low-mass region is effective only for the singlet-doublet two-component DM in the mass regime $m_\phi < m_{H^0}$.

[5]The scenario $m_{H^0} > 2m_\phi$ is equivalent to the complex singlet scalar DM model [8–10], as the presence of H_2 does not affect the ϕ abundance because the semi-annihilation processes become inefficient.

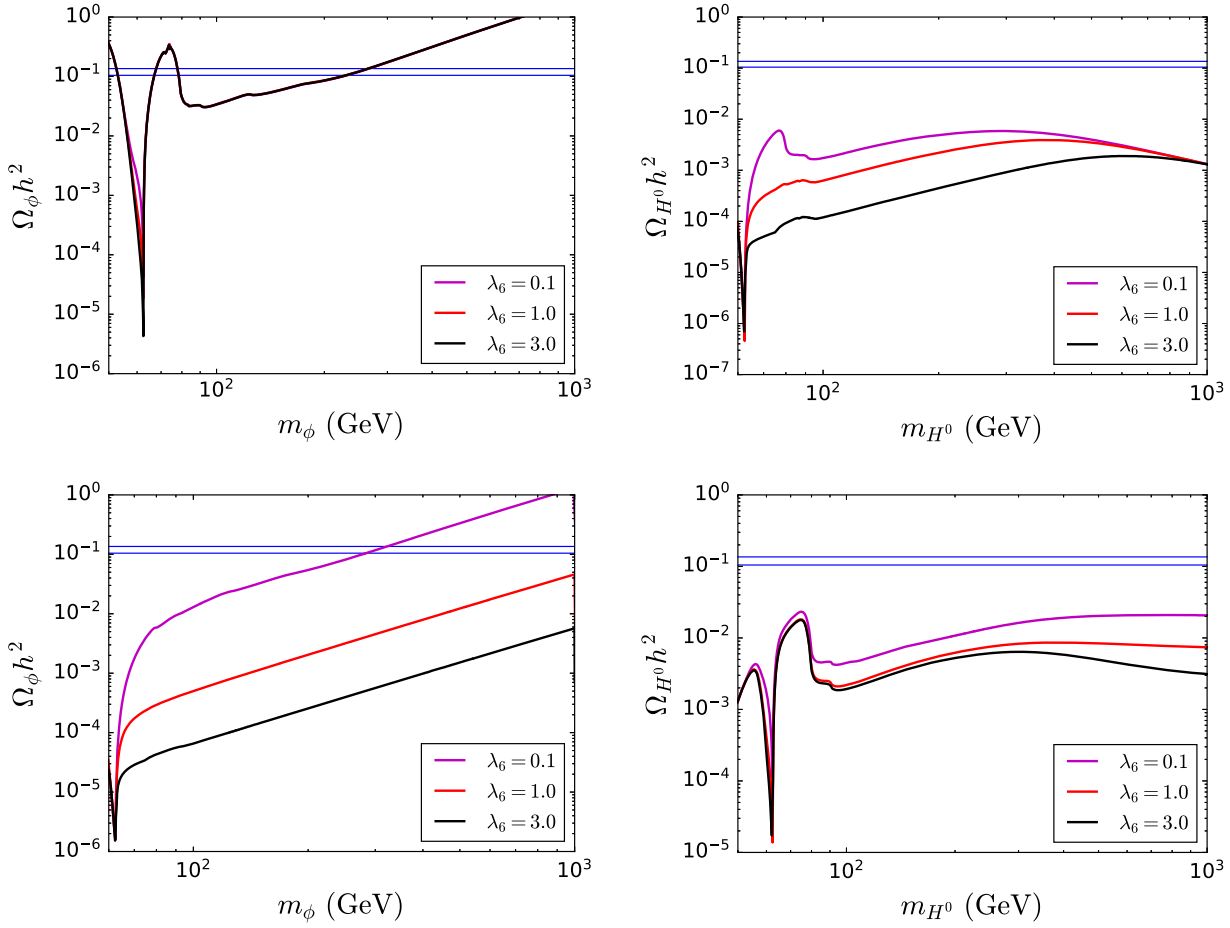

FIG. 3. Effect of λ_6-mediated DM conversion on Ω_ϕ and Ω_{H^0} for $m_{H^0}/m_\phi = 1.2$ (top panels) and $m_\phi/m_{H^0} = 1.2$ (bottom panels). In each plot $m_{H^\pm}/m_{H^0} = 1.1$, $\lambda_7 = 0$ and $\lambda_8 = \lambda_L = 0.1$ have been set.

B. DM direct detection

Elastic scattering of the DM particles off nuclei can take place since both ϕ and H^0 couple to quarks by the exchange of a Higgs boson, and also by the exchange of a Z boson for the case of H^0, as displayed in Fig. 6. The SI DM-nucleon scattering cross section $\sigma^{\rm SI}_{\chi N}$ (for a target nucleus with atomic and mass numbers $\mathcal{Z}$ and $\mathcal{A}$) is given by [70]

$$\sigma^{\rm SI}_{\chi N} = \frac{1}{\pi}\left[\frac{\mu_{\chi p}\mathcal{Z}(f^S_{\chi p}+f^V_{\chi p})+\mu_{\chi n}(\mathcal{A}-\mathcal{Z})(f^S_{\chi n}+f^V_{\chi n})}{\mathcal{A}}\right]^2, \tag{11}$$

where the $f^{S(V)}_{\chi\alpha}$ coefficients correspond to the scalar (vector) DM couplings to protons ($\alpha = p$) and neutrons ($\alpha = n$), whereas $\mu_{\chi\alpha}$ denotes the respective DM-nucleon reduced masses, and $\chi = \phi, H^0$. The Higgs effective couplings are given by

$$f^S_{\chi\alpha} = -\lambda_{\chi h}\frac{m_\alpha f_\alpha}{m_h^2 m_\chi}, \tag{12}$$

with $f_{p,n} \approx 0.3$ denoting the quark content of nucleons, $\lambda_{\phi h} = \lambda_8$ and $\lambda_{H^0 h} = 2\lambda_L$. Since for ϕ the Z-mediated interaction with nucleons is not allowed, it turns out that $f^V_{\phi\alpha} = 0$ for $\alpha = p, n$, whereas for H^0 we have

$$f^V_{H^0\alpha} = \begin{cases} -\left(1-4s^2_W\right)\frac{G_F}{\sqrt{2}}, & \alpha = p, \\ \frac{G_F}{\sqrt{2}}, & \alpha = n. \end{cases} \tag{13}$$

Because the weak-isospin charge of H^0, it presents large scattering rates for typical values of the model parameters. For instance, with $|\lambda_L| < 3$ and $m_{H^0} \gtrsim 100$ GeV, it is found that [16]

$$\sigma^{\rm SI}_{H^0 N} \approx \frac{G_F^2}{2\pi}\frac{\mu_N^2}{\mathcal{A}^2}[(\mathcal{A}-\mathcal{Z})-\mathcal{Z}(1-4s^2_W)]^2 \approx 2\times 10^{-3}\ \text{pb}. \tag{14}$$

To understand this, let us recall that the Z couplings are proportional to $T_3\cos^2\theta_W - (Y/2)\sin^2\theta_W$, being θ_W the Weinberg mixing angle, T_3 the third weak-isospin

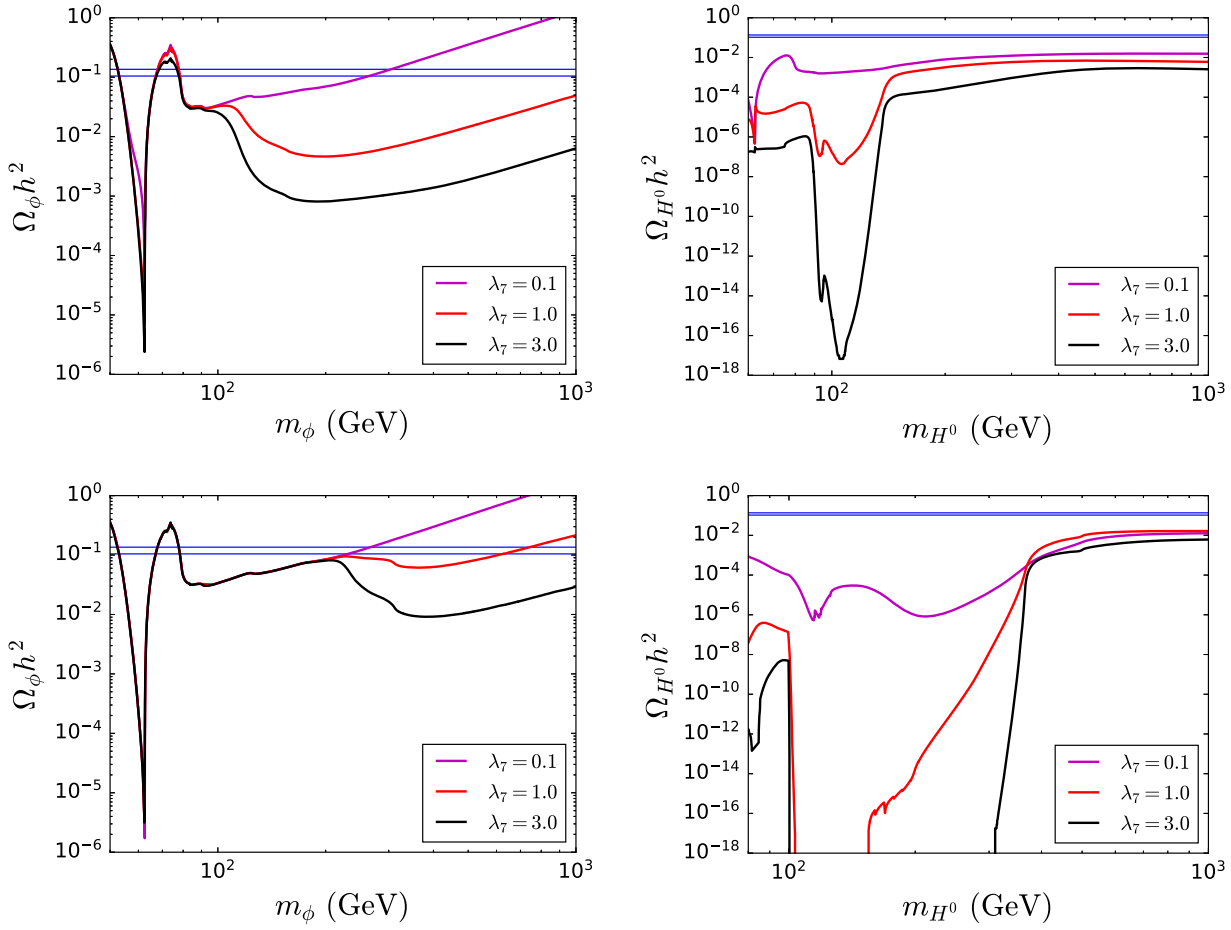

FIG. 4. Effect of λ_7-mediated DM semi-annihilation on Ω_ϕ and Ω_{H^0} for two different values of m_{H^0}/m_ϕ; 1.2 (top panels) and 1.6 (bottom panels). In all panels $m_{H^\pm}/m_{H^0} = 1.1$, $\lambda_6 = 0$ and $\lambda_8 = \lambda_L = 0.1$ have been set.

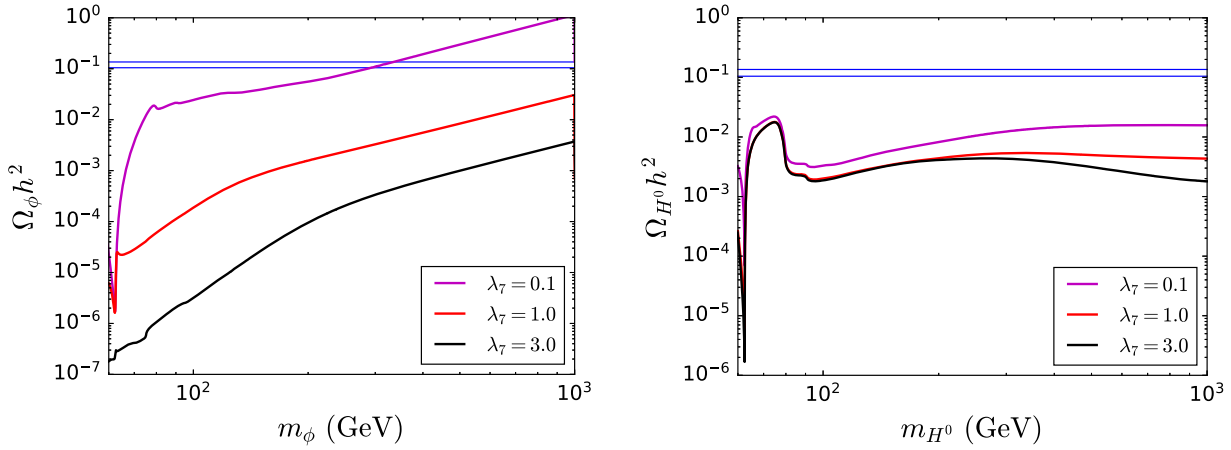

FIG. 5. Effect of λ_7-mediated DM semi-annihilations on Ω_ϕ and Ω_{H^0} for $m_\phi/m_{H^0} = 1.2$. Larger values of m_ϕ/m_{H^0} do not lead to significant variations of Ω_ϕ or Ω_{H^0}. We take $m_{H^\pm}/m_{H^0} = 1.1$, $\lambda_6 = 0$, and $\lambda_8 = \lambda_L = 0.1$.

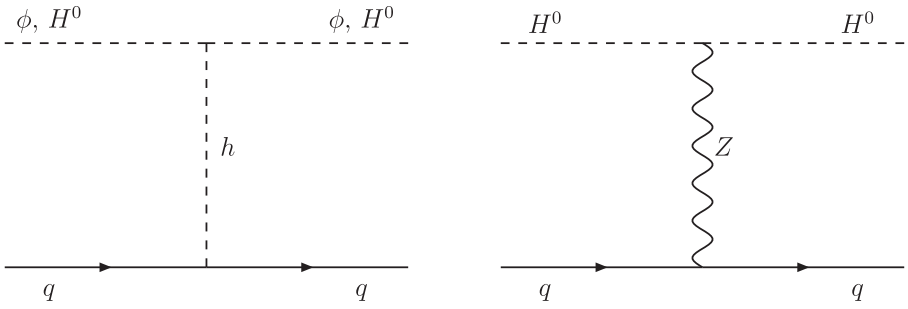

FIG. 6. Feynman diagrams for the elastic scattering of DM particles with nuclei mediated by the Higgs (left panel) and Z bosons (right panel).

component and Y the SM hypercharge. For H^0, $T_3 = -1/2$ and $Y = 1$. The fact that $Y \neq 0$ induces unsuppressed vector interactions with the Z boson which give rise to an elastic SI cross section between H^0 and the nucleons that is several orders of magnitude above the current upper bounds.[6]

In multicomponent DM scenarios, the quantity to be compared against the DD limits provided by experimental collaborations is not merely the cross section itself. Instead, it is the expression $\Omega_\chi \sigma^{\rm SI}_{\chi N}/\Omega_{\rm DM}$, where $\Omega_{\rm DM}$ represents the total observed DM abundance. To remain below the current upper bounds, the relic density of H^0 must be suppressed by at least six orders of magnitude. This suppression is precisely noticed in the mass hierarchy $m_\phi < m_{H^0}$, particularly when semi-annihilation processes are significant (see the previous section).

In order to determine the DD constraints on this two-component DM model, we determine the expected total number of events $\mathcal{N}_{\rm events}$ in a experiment such as XENON [20], PANDAX [18], and LZ [19]. This can be calculated through the expression [71],

$$\mathcal{N}_{\rm events} = \omega_{\rm exp} \int_{\mathcal{S}_{\rm min}}^{\mathcal{S}_{\rm max}} d\mathcal{S} \sum_{n=1}^{\infty} {\rm Gauss}(\mathcal{S}|n, \sqrt{n}\sigma_{PMT}) \times \int_0^\infty dE_R \epsilon(E_R) {\rm Poiss}(n|\nu(E_R)) \frac{dR}{dE_R}, \tag{15}$$

where $\omega_{\rm exp}$ is the exposure, $\mathcal{S}$ denotes the number of photoelectrons (PE) resulting from the collision between a WIMP particle and a target nucleus. σ_{PMT} is the average single-PE resolution of the photomultipliers arranged inside the detector to measure the scintillation photons (signal S1) resulting from the collisions. $\epsilon(E_R)$ is the detection efficiency and $\nu(E_R)$ is the expected number of PEs for a given recoil energy E_R. As for dR/dE_R, it represents the differential recoil rate per unit of detector mass. In the current scenario, this rate comes given by the sum of the rates associated with each component particle [72,73],

$$\frac{dR}{dE_R} = \frac{dR_\phi}{dE_R} + \frac{dR_{H^0}}{dE_R}, \tag{16}$$

with

$$\frac{dR_\chi}{dE_R} = \frac{1}{2} \frac{\rho_\chi \sigma_{\chi T}}{m_\chi \mu^2_{\chi T}} F^2(E_R) \mathcal{H}(E_R, m_\chi). \tag{17}$$

Here $\rho_\chi \equiv (\Omega_\chi/\Omega_{\rm DM})\rho_\odot$ stands for the contribution of the χ-component to the local DM density $\rho_\odot$ (≈ 0.3 GeV/cm^3), $\sigma_{\chi T}$ and $\mu_{\chi T}$ are, respectively, the scattering cross section and the reduced mass of the χ-nucleus system, while $F^2(E_R)$ is the recoil-energy dependent nuclear form factor given by [74,75]

$$F^2(E_R) = \left[3\frac{j_1(qR)}{qR}\right]^2 e^{-q^2 s^2}, \tag{18}$$

where j_1 is the spherical Bessel function of the first kind, $q = \sqrt{2 m_T E_R}$ and $R = \sqrt{c^2 + \frac{7}{3}\pi^2 a^2 - 5s^2}$, with $c = (1.23A^{1/3} - 0.6)$ fm, $a = 0.52$ fm and $s = 0.9$ fm. On the other hand,

$$\mathcal{H}(E_R, m_\chi) = \int_{v_{\rm min}}^\infty \frac{f_\oplus(\mathbf{v}_{\rm rel})}{v_{\rm rel}} d^3\mathbf{v}_{\rm rel}, \tag{19}$$

$f_\oplus$ being the astrophysical DM velocity distribution measured with respect to the lab frame and $v_{\rm min}$ the minimum speed needed to produce a recoil with energy E_R,

$$v_{\rm min}(E_R, m_\chi) = \sqrt{\frac{(m_\chi + m_T)^2 E_R}{2 m_\chi^2 m_T}}. \tag{20}$$

Regarding the galactic frame, and assuming the so-called Standard Halo Model [76,77], these velocities follow a Maxwell-Boltzmann distribution of the form,

[6]One way to relax these constraints is to allow a mass splitting between the CP-even and CP-odd components of at least ~100 keV, since this kinematically disfavors the interaction through the Z portal, reducing to nonsignificant inelastic collisions. In the current model, however, such a scenario is not possible due to the Z_6 symmetry.

$$f(\mathbf{v}) = \begin{cases} \frac{1}{N} e^{-|\mathbf{v}|^2/v_0^2}, & \text{for } |\mathbf{v}| < v_{\text{esc}}, \\ 0, & \text{for } |\mathbf{v}| > v_{\text{esc}}, \end{cases} \tag{21}$$

with galactic escape velocity v_{esc} (∼540 km/s), velocity dispersion v_0 (∼220 km/s) [78][7] and normalization

$$N = \pi^{3/2} v_0^3 \left[\text{erf}\left(\frac{v_{\text{esc}}}{v_0}\right) - \frac{2 v_{\text{esc}}}{\sqrt{\pi} v_0} e^{-\left(\frac{v_{\text{esc}}}{v_0}\right)^2} \right]. \tag{22}$$

Thus, if $\mathbf{v}_E$ is the Earth's velocity with respect to the galactic frame (∼232 km/s [78]), then $f_\oplus(\mathbf{v}_{\text{rel}}) = f(\mathbf{v}_{\text{rel}} + \mathbf{v}_E)$. Finally, due to the scalar nature of the DM candidates, the particle-physics dependent observable $\sigma_{\chi T}$ can be written in terms of the SI χ-nucleon scattering cross section $\sigma^{\text{SI}}_{\chi N}$ as

$$\sigma_{\chi T} = \left(\mathcal{A} \frac{\mu_{\chi T}}{\mu_{\chi N}} \right)^2 \sigma^{\text{SI}}_{\chi N}. \tag{23}$$

Putting it all together, we can express the number of events predicted by the model in DD experiments as the sum of the events induced by the singlet and those generated by the doublet, i.e.,

$$\mathcal{N}_{\text{events}} = \mathcal{N}^{\phi}_{\text{events}} + \mathcal{N}^{H^0}_{\text{events}}, \tag{24}$$

where each contribution is proportional to the product of the corresponding local relic density ρ_χ and the SI scattering cross section with nucleons $\sigma^{\text{SI}}_{\chi N}$, as indicated in Eqs. (17) and (23).

III. NUMERICAL ANALYSIS

In this section we investigate the phenomenological implications of the constraints on the model and establish the regions of the parameter space where semi-annihilation processes render it viable.

A. Theoretical constraints

1. Perturbativity

To guarantee that tree-level corrections are always more relevant than the one-loop contributions, we demand vertex factors to be less than 4π in the Feynman rules associated with the quartic interactions [79]. If several upper bounds for a same coupling are possible, the most stringent one is chosen. The corresponding upper bounds are given by

$$\lambda_2 < \frac{2\pi}{3}, |\lambda_3| < 4\pi, |\lambda_3 + \lambda_4| < 4\pi, |\lambda_4| < 8\pi, |\lambda_8| < 4\pi, |\lambda_6| < 4\pi, |\lambda_\phi| < \pi. \tag{25}$$

2. Perturbative unitarity

When the energy involved in a scalar-scalar scattering process is high enough in comparison with the masses of the involved particles, all the contributions to the tree-level scattering matrix mediated by propagators are negligible so that only quartic point interactions are relevant. In this limit the s-wave scattering amplitudes must satisfy the perturbative unitarity condition, which results in the fact that the eigenvalues of the scattering matrices must all be less than 8π [80]. The unitarity bounds for the current model can be obtained from the general analysis reported in Ref. [81]. When the initial scattering states are classified according to the total hypercharge Y, weak isospin T_3 and discrete Z_6 charge, the $S^Y_{T_3}$ scattering matrices can be expressed as

$$8\pi S^2_1 = \begin{pmatrix} 2\lambda_1 & 0 & 0 \\ 0 & 2\lambda_2 & 0 \\ 0 & 0 & \lambda_3 + \lambda_4 \end{pmatrix}, \qquad 8\pi S^2_0 = \lambda_3 - \lambda_4, \tag{26}$$

$$8\pi S^1_{1/2} = \begin{pmatrix} \lambda_6 & \lambda_7 & 0 & 0 \\ \lambda_7 & \lambda_8 & 0 & 0 \\ 0 & 0 & \lambda_8 & 0 \\ 0 & 0 & 0 & \lambda_6 \end{pmatrix}, \qquad 8\pi S^0_1 = \begin{pmatrix} 2\lambda_1 & \lambda_4 & 0 & 0 \\ \lambda_4 & 2\lambda_2 & 0 & 0 \\ 0 & 0 & \lambda_3 & 0 \\ 0 & 0 & 0 & \lambda_3 \end{pmatrix}, \qquad 8\pi S^0_0 = \begin{pmatrix} A_{3\times 3} & 0_{3\times 4} \\ 0_{4\times 3} & B_{4\times 4} \end{pmatrix}, \tag{27}$$

where

[7]For simplicity, we assume that these parameters are the same for both DM components. A more general analysis with different dispersion velocities was carried out in Refs. [72,73].

$$A_{3\times3}=\begin{pmatrix}6\lambda_1 & 2\lambda_3+\lambda_4 & \sqrt{2}\lambda_8\\ 2\lambda_3+\lambda_4 & 6\lambda_2 & \sqrt{2}\lambda_6\\ \sqrt{2}\lambda_8 & \sqrt{2}\lambda_6 & \lambda_\phi\end{pmatrix},\qquad B_{4\times4}=\begin{pmatrix}\lambda_\phi & 0 & \lambda_7 & 0\\ 0 & \lambda_\phi & 0 & \lambda_7\\ \lambda_7 & 0 & \lambda_3+2\lambda_4 & 0\\ 0 & \lambda_7 & 0 & \lambda_3+2\lambda_4\end{pmatrix}. \tag{28}$$

3. Vacuum stability

Vacuum stability demands a scalar potential bounded from below. To establish the corresponding conditions, we consider as usual high field values so that only quartic terms are relevant, and build the quartic interaction matrix in terms of non-negative field variables in the following way [82]:

$$|H_1|^2=r_1^2,\qquad |H_2|^2=r_2^2,$$
$$H_1^\dagger H_2=r_1r_2\rho e^{i\theta},\qquad \phi=r_\phi e^{i\theta_\phi}. \tag{29}$$

Here $r_1=r\cos\gamma$ and $r_2=r\sin\gamma$, with $r,r_\phi\geq0$ and $0\leq\gamma\leq\pi/2$, whereas $|\rho|\leq1$ and $\theta,\theta_\phi\in[0,2\pi]$. The necessary and sufficient stability conditions are obtained by demanding this matrix to be copositive [83]. For the Z_6 model discussed here, the conditions are [81]

$$\lambda_{\phi,1,2}>0,\qquad \lambda_3+2\sqrt{\lambda_1\lambda_2}>0,$$
$$\lambda_3+\lambda_4+2\sqrt{\lambda_1\lambda_2}>0,\qquad \sqrt{\Lambda_{11}\Lambda_{22}}+\Lambda_{12}>0, \tag{30}$$

with

$$\Lambda_{11}=\lambda_1\cos^4\gamma+(\lambda_3+\lambda_4\rho^2)\cos^2\gamma\sin^2\gamma+\lambda_2\sin^4\gamma, \tag{31}$$

$$\Lambda_{22}=\lambda_\phi, \tag{32}$$

$$\Lambda_{12}=\frac{1}{2}[\lambda_8\cos^2\gamma+\lambda_7\rho\cos\gamma\sin\gamma\cos(\theta-2\theta_\phi)+\lambda_6\sin^2\gamma]. \tag{33}$$

These conditions must be fulfilled for all defined values of ρ, γ, θ, and θ_ϕ.

4. Renormalization group equations

We determine the evolution with energy of all dimensionful and dimensionless parameters by solving the two-loop renormalization group equations (RGEs) obtained with SARAH [84,85], and checking that the conditions of perturbative unitarity and vacuum stability, as well as perturbativity are satisfied for the different values of the energy scale Λ. To determine the viable parameter space we only consider points for which all the theoretical conditions are guaranteed up to energy scales above the highest mass present in the dark sector, which is $m_{H^\pm}$ in the present setup.

B. Experimental constraints

1. EW precision tests

The new scalar fields may modify the vacuum polarization of the gauge bosons. These effects are parameterized by the so-called EW oblique parameters S, T, and U [86]. The SM best-fit reads $\bar{S}=0.06\pm0.09$, $\bar{T}=0.10\pm0.07$ with a correlation coefficient $+0.91$ (under the assumption $U=0$) [87]. In the present model the new contributions to S and T are given by [16]

$$S=-\frac{\ln(r)}{6\pi},\qquad T=\frac{m_{H^0}^2}{16\pi m_W^2 s_W^2}\frac{r^4-1-4r^2\ln r}{r^2-1}, \tag{34}$$

where $r=m_{H^\pm}/m_{H^0}$, m_W is the W-boson mass and $s_W^2=0.223$. An agreement with the EW precision tests is maintained as long as the splitting between the masses of the H^0 and $H^\pm$ is small.

2. Collider constraints

For the diphoton channel, the signal strength $R_{\gamma\gamma}$ measures the ratio of the observed diphoton production cross section relative to the SM expectation [88],

$$R_{\gamma\gamma}=\frac{\sigma(pp\to h\to\gamma\gamma)^{Z_6}}{\sigma(pp\to h\to\gamma\gamma)^{\rm SM}}=\frac{\sigma(pp\to h\to\gamma\gamma)^{\rm IDM}}{\sigma(pp\to h\to\gamma\gamma)^{\rm SM}}$$
$$\approx\frac{[{\rm Br}(h\to\gamma\gamma)]^{\rm IDM}}{[{\rm Br}(h\to\gamma\gamma)]^{\rm SM}}. \tag{35}$$

This observable was measured by ATLAS [89] and CMS [90] with 139 fb^{-1} obtaining $R_{\gamma\gamma}^{\rm ATLAS}=1.03\pm0.12$ and $R_{\gamma\gamma}^{\rm CMS}=1.12\pm0.09$. The impact of the Z_6-odd charged scalars over the decay ratio can be quantified from Ref. [91] as

$$R_{\gamma\gamma}=\left|1+\frac{1}{A_{\rm SM}}\left[\frac{\lambda_3v^2A_S(\tau_{H^\pm})}{2m_{H^\pm}^2}\right]\right|^2, \tag{36}$$

where $A_{\rm SM}=-6.5$ is the SM contribution from charged fermions and gauge bosons, $\tau_{H^\pm}=m_h^2/(4m_{H^\pm}^2)$ and $A_S(\tau)=-[\tau-\arcsin^2(\sqrt{\tau})]/\tau^2$.

The LHC also sets bounds on the invisible Higgs decays. If one or both DM particles are lighter than half the Higgs mass, the $h\to\chi^*\chi$ decay would be allowed, contributing to the invisible branching ratio of the Higgs boson, $\mathcal{B}_{\rm inv}$. The decay width associated with these processes is given by

$$\Gamma(h \to \chi^* \chi) = \frac{\lambda_\chi^2 v^2}{16\pi m_h}\left[1 - \frac{4m_\chi^2}{m_h^2}\right]^{1/2}, \tag{37}$$

with $\lambda_\chi = \lambda_8$ for $\chi = \phi$, and $\lambda_\chi = 2\lambda_L$ for $\chi = H^0$. To be consistent with current data, we require $\mathcal{B}_{\text{inv}} \leq 0.13$ [92,93].

On the other hand, Large Electron–positron Collider sets limits on the masses of all charged particles which can be directly produced, as well as on particles resulting from their decays. These limits can be easily reinterpreted for the new scalars present in the model. The decays of gauge bosons into Z_6-odd pairs are excluded by their invisible width measurements [94], leading to the constraints,

$$m_{H^0} + m_{H^\pm} > m_W, \qquad m_{H^0, H^\pm} > \frac{m_Z}{2}. \tag{38}$$

Direct chargino searches at Large Electron–Positron Collider II can also be reinterpreted for the search of charged scalars [95], leading to $m_{H^\pm} > 70$ GeV. For a compressed spectra, a tighter constraint applies, namely $m_{H^\pm} > 100$ GeV.

3. Dark matter constraints

Since both ϕ and H^0 constitute all the DM present in the universe, their abundances must satisfy the condition,

$$\Omega_\phi + \Omega_{H^0} = \Omega_{\text{DM}}, \tag{39}$$

with Ω_{DM} denoting the total observed DM abundance as measured by the Planck Collaboration [1] $\Omega_{\text{DM}}h^2 = 0.1198 \pm 0.0012$. Given that the theoretical prediction on the relic density is not expected to be as precise as that of Planck, in our scans we consider a model compatible with that value if the DM abundance, as determined by micrOMEGAs, lies between 0.11 and 0.13, which amounts to about a 10% uncertainty. In what follows, we denote the fraction of the total DM density accounted for by each component as

$$\xi_\chi \equiv \frac{\Omega_\chi}{\Omega_{\text{DM}}}, \qquad \chi = \phi, H^0, \tag{40}$$

so that $\xi_\phi + \xi_{H^0} = 1$.

Given that currently the strongest DD constraints are those reported by the LZ Collaboration with an exposure of 60.0 days and a fiducial mass of 5.5 tons of liquid xenon ($\mathcal{A} = 131$, $\mathcal{Z} = 54$, and $m_T = 122.0$ GeV) [19], we consider the characteristics and specifications of this detector to determine $\mathcal{N}_{\text{events}}$ from Eq. (15). For this goal, we take $\mathcal{S}$ between 3 PE and 80 PE [19] and fix $\sigma_{PMT} = 0.4$ according to Ref. [96], whereas $\epsilon(E_R)$ is read from the black solid line of Fig. 2 in Ref. [19]. From the S_1 yield given in the upper left panel of Fig. 2 in Ref. [97] we can extract $\nu(E_R)$ since this corresponds to $\nu(E_R)/E_R$.

With the aid of a test statistic (TS), it is possible to obtain an upper bound for $\mathcal{N}_{\text{events}}$. Closely following Ref. [98], we take

$$\text{TS}(m_\chi) = -2\ln\left[\frac{\mathcal{L}(\mathcal{N}_{\text{events}})}{\mathcal{L}_{\text{BG}}}\right], \tag{41}$$

with

$$\mathcal{L}(\mathcal{N}_{\text{events}}) = \frac{(\mathcal{N}_{\text{events}} + \mathcal{N}_{BG})^{\mathcal{N}_{\text{obs}}}}{\mathcal{N}_{\text{obs}}!} e^{-(\mathcal{N}_{\text{events}} + \mathcal{N}_{\text{BG}})}, \tag{42}$$

and $\mathcal{L}_{\text{BG}} \equiv \mathcal{L}(0)$. Here $\mathcal{N}_{\text{obs}}$ and $\mathcal{N}_{\text{BG}}$ stand for, respectively, the number of observed and background events. By requiring $\text{TS}(m_\chi) > 2.71$, 90% CL limits can be obtained. With $\mathcal{N}_{\text{obs}} = 0$ and $\mathcal{N}_{\text{BG}} = 333$ [99], the expected number of events must fulfill $\mathcal{N}_{\text{events}} \lesssim 31$. This bound will be used to constrain the free parameters of the model.

Furthermore, to gain insight into the parameter space regions within the projected sensitivities of planned experiments, we consider LZ with a full exposure $\omega_{\text{exp}} = 15.33$ ton · yr [100] and apply the maximum gap method assuming zero observed events [101]. In this hypothetical scenario, we require $1 - \exp(-\mathcal{N}_{\text{events}}) \geq 0.9$, which implies $\mathcal{N}_{\text{events}} \lesssim 2.3$.

C. Scan

To explore the viability of the model, we conducted a random scan over the new particle masses and the free scalar couplings and determined the parameter space regions in which all constraints imposed on the model are satisfied. Specifically, these parameters are allowed to randomly vary as

$$40\ \text{GeV} \leq m_\phi \leq 1000\ \text{GeV}, \qquad m_\phi < m_{H^0} < 2m_\phi,$$
$$m_{H^0} < m_{H^\pm} \leq 2\ \text{TeV}, \tag{43}$$

$$10^{-4} \leq \lambda_2 < \frac{2}{3}\pi, \qquad 10^{-4} \leq \lambda_\phi < \pi,$$
$$10^{-4} \leq |\lambda_3|, |\lambda_8|, |\lambda_6|, |\lambda_7| < 4\pi. \tag{44}$$

Some of the observables, as DM abundances, rates of ID processes and the Higgs invisible decay width, were numerically determined by means of the micrOMEGAs whereas others were calculated analytically.

D. Results

The resulting viable parameter space projected onto different planes is displayed in Fig. 7. The red points correspond to those where the upper bound on the expected number of events in the LZ experiment is satisfied, while the black points denote those that would be excluded with a full exposure of 15.33 ton · year if no events are observed. The most significant conclusion drawn from this figure is that, thanks to the semi-annihilation processes, it is possible to satisfy stringent DD bounds with DM masses around the EW scale. As can be seen from the top panels, λ_7 must be

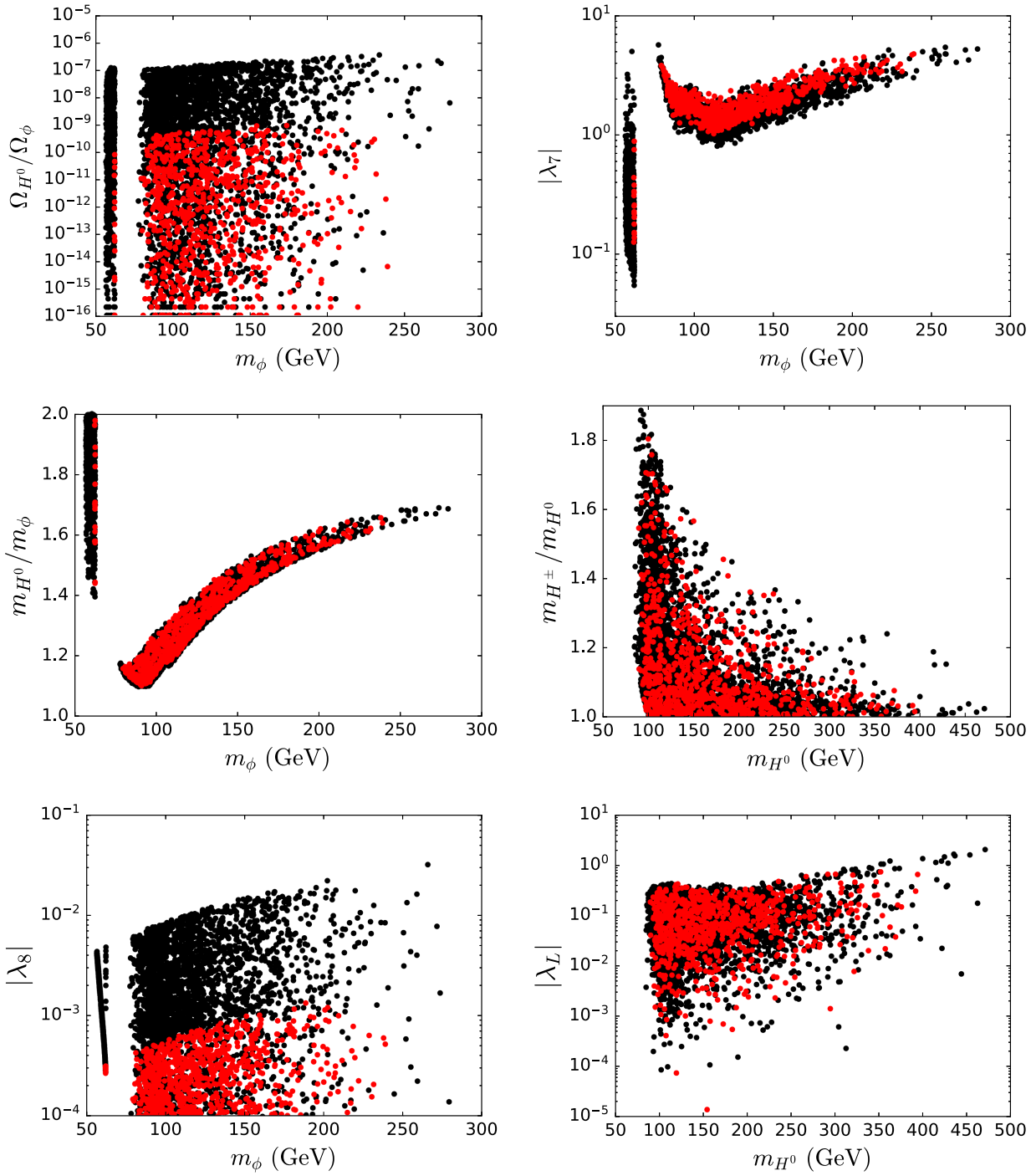

FIG. 7. Parameter space of the model. On the left (right), the mass ratio m_{H^0}/m_ϕ ($m_{H^\pm}/m_{H^0}$) is shown as a function of the ϕ (H^0) mass. The ratio of the DM relic abundances as a function of m_ϕ also is displayed. Scalar couplings λ_7 and λ_8 (λ_L) are shown in terms of the ϕ (H^0) mass.

large enough ($\lambda_7 \gtrsim 1$) to provide the sufficient suppression on Ω_{H^0} (at least seven orders of magnitude with respect to $\Omega_\phi \approx \Omega_{\rm DM}$)[8] and lead to a small contribution to $\Omega_{\rm DM}$. In this way, for the setup considered in this work, the lightest component ϕ constitutes the bulk of the DM content of the Universe.

The center panels show that the viable models involve DM masses ranging from the Higgs resonance up to approximately 280 GeV for the singlet component (left panel), and

[8] λ_6 is hardly constrained meaning that the conversion processes are not relevant on setting the DM relic abundances.

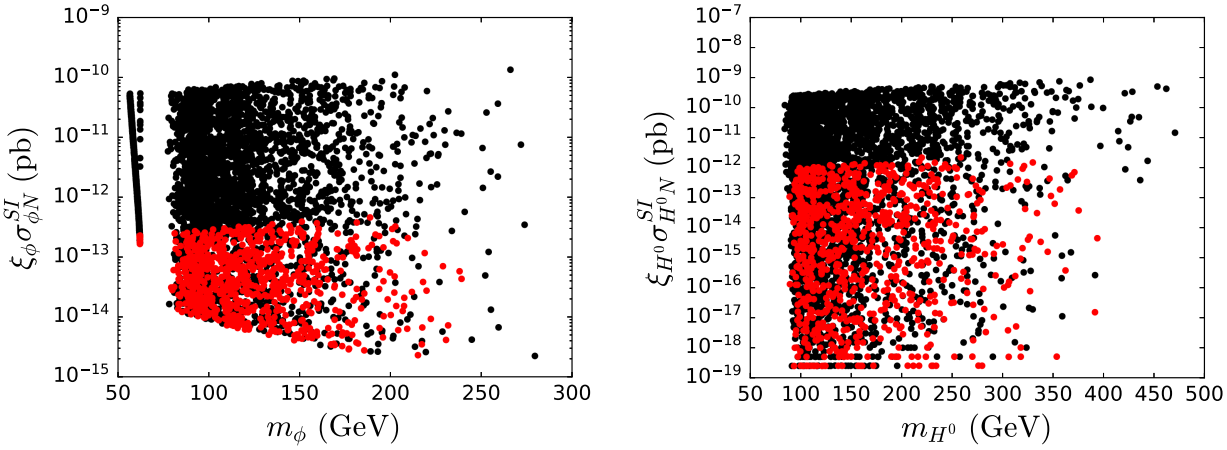

FIG. 8. SI cross sections for elastic scattering of ϕ (left panel) and H^0 (right panel) with nuclei scaled by ξ_ϕ and ξ_{H^0}, respectively.

from just over 90 GeV to around 480 GeV for the doublet component (right panel). The low-mass region (∼40 GeV) is excluded by Higgs and collider physics. It is important to highlight that the DM masses do not need to be degenerated. As for the charged and neutral doublet components, the mass splitting between them is strongly constrained by the EW precision tests and decreases with m_{H^0} (right panel).

The Higgs portal couplings with the singlet (λ_8) and the doublet (λ_L) are displayed in the bottom panels. λ_L is not as constrained as λ_8, as it can take values as small as the lower bound defined in the scan (10^{-4}) and as large as ∼1. This is because, although the H^0-nuclei scattering cross-section depends explicitly on λ_L, it is completely dominated by the Z portal, rendering irrelevant the effect of the Higgs portal in such a case. In contrast, λ_8 is constrained to below 0.01 due to its effect on the expected events in LZ. This upper limit would be tightened by almost an order of magnitude under the most conservative scenario of the future LZ setup. It is worth noting that the expected number of events in DD experiments has two contributions, one due to ϕ and another to H^0, both proportional to the product of their respective local relic densities and scattering cross sections with nuclei. Thus, to fulfill a more stringent future bound on $\mathcal{N}_{\text{events}}$, a decrease of the magnitude of λ_8 is necessary, thus reducing the event fraction associated with ϕ.

At first glance, it might seem then that the model considered is basically a one-component DM model, given the almost negligible contribution of H^0 to the total DM relic density. Nevertheless, the compensation between the very large Z coupling of H^0 and its very small relic density makes the fraction of scattering events associated with H^0 to be small enough to satisfy the limits on $\mathcal{N}_{\text{events}}$ and at the same time large enough for sizable signals to be possible (see Fig. 8). In fact, $\mathcal{N}^{H^0}_{\text{events}}$ can be equal or even greater than the singlet contribution $\mathcal{N}^{\phi}_{\text{events}}$. The most conservative prospects for the future LZ commissioning shows, for instance, that a significant portion of the models that would be excluded (black points not overlapping with the red ones in Fig. 8) are characterized by a greater proportion ($\gtrsim$70%) of expected events associated with H^0. In this way, we see that either or even both DM particles are susceptible to detection in future searches.

To understand these results, let us recall that the strong constraints on Higgs- and Z-portal models like the one considered arise due to the tension between efficient DM annihilation in the early universe, which requires large λ_8 and λ_L couplings, and the bounds on DM-nuclei scattering cross sections, which demand small values of these couplings. In this model, however, this tension is relaxed due to the presence of the λ_7 interaction, which induces semi-annihilation processes during the freeze-out. These processes contribute to reduce the relic abundances of ϕ and H^0 without the need for large Higgs couplings or large DM masses. Such a relaxation allows us then to conclude that the effects introduced by the Z_6 symmetry enable a scenario capable of satisfying, for DM masses at the EW scale, the stringent experimental restrictions. Contrary to what is usually assumed in the literature, a scalar DM model in which the Z-portal interactions are relevant (and even dominant) can be perfectly viable, thanks to semi-annihilations which naturally arise in a multicomponent DM framework.

Regarding DM indirect searches, the most relevant annihilation signals originate from the semi-annihilation channels $\phi\phi \to H^0 Z$ and $\phi\phi \to H^{\pm} W^{\mp}$, with rates as large as 10^{-25} cm^3/s. As there are no dedicated studies addressing ID through semi-annihilations in multicomponent DM scenarios, we just display the corresponding rates scaled by ξ^2_ϕ in Fig. 9. As a result, it remains unclear whether forthcoming observations will explore the viable parameter space of this model. This uncertainty underscores the need for a focused study to reach definitive conclusions.

A final comment is in order with respect to scenarios featuring larger $SU(2)_L$ multiplets with nonvanishing hypercharge. Firstly, let us consider an $SU(2)_L$ multiplet H_n of dimension $n > 2$, as opposed to a doublet. Should ϕ

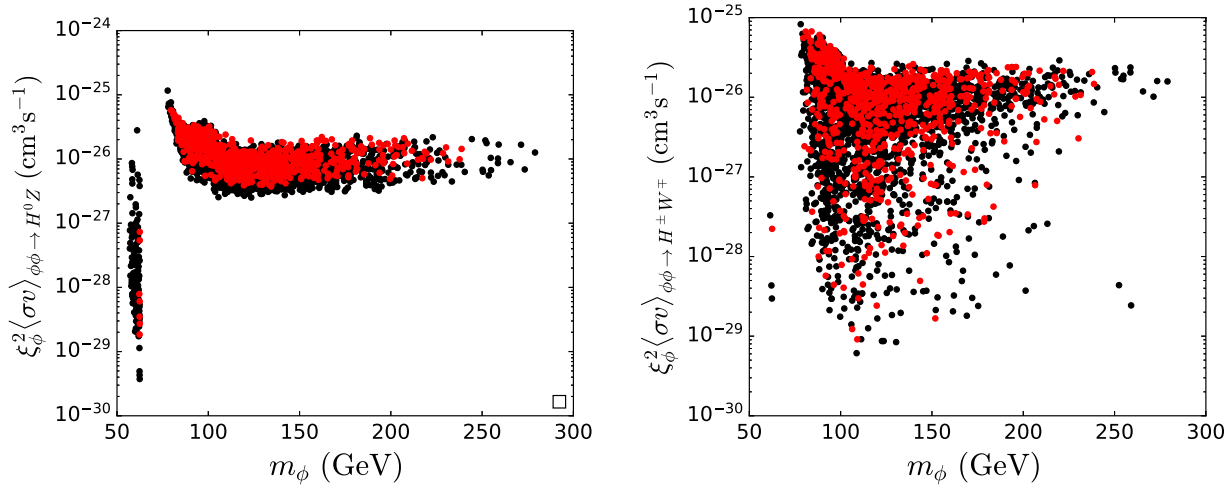

FIG. 9. Most relevant semi-annihilation processes for ID searches. Scaled cross sections are shown for $\phi\phi \to H^0 Z$ (left panel) and $\phi\phi \to H^\pm W^\mp$ (right panel).

remain a singlet, an important observation emerges; the operator $\mathcal{O}_n = H_n^{(\dagger)} H_1 \phi^2$ is no longer invariant under $SU(2)_L$. Therefore, the two-component scalar scenario having a singlet and a multiplet larger than a doublet does not present semi-annihilation processes of the type $\mathcal{O}_n$. Next, we go through the case where the singlet field is promoted to a $SU(2)_L$ multiplet ϕ_m of dimension $m > 1$ with the same hypercharge of the singlet ϕ, that is $Y(\phi_m) = 0$, which in turn demands that m is odd [102,103]. The corresponding operator associated with semi-annihilations takes the form $\mathcal{O}_{nm} = H_n^\dagger H_1 \phi_m^2$, and is gauge invariant for n even and $Y(H_n) = 1$. These (m, n) scenarios resemble to some extent the singlet-doublet two-component model when the neutral component of ϕ_m, ϕ_m^0, becomes the lightest candidate, and the second candidate being the neutral particle with tree-level Z interactions associated with H_n, H_n^0. However, thermal relics belonging to higher multiplets possess very large masses, usually in the range of several TeV [103,104], indicating that the exponential suppression on $\Omega_{H_n^0}$ would not be enough efficient to attenuate the DD rates of H_n^0.

IV. CONCLUSIONS

In this work, we demonstrated that in multicomponent scenarios featuring a scalar doublet candidate with unsuppressed vectorlike neutral-current gauge interactions with the Z boson, the Z-portal can still be open because of the effect of the semi-annihilation processes on the relic abundance on such a candidate. For this goal, we enlarged the SM scalar sector with a second Higgs doublet H_2 and a complex singlet ϕ, both with vanishing vacuum expectation value. A Z_6 symmetry prevents the commonly invoked mass splitting of the real and imaginary components of the neutral member of the doublet, H_0. As a result, it remains complex, leading to a two-component scalar DM scenario with semi-annihilation processes induced by the interaction term $H_2^\dagger H_1 \phi^2$.

We have shown that these semi-annihilations drastically reduce the relic abundance of H^0 by at least seven orders of magnitude relative to that of ϕ, implying that the ϕ component accounts for almost all of the observed DM in the Universe. However, the smallness of Ω_{H^0} counteracts the effect of the Z-mediated elastic scattering between H^0 particles and nuclei, making signatures from H^0 elusive enough to satisfy the most stringent current limits while remaining detectable in ongoing and future DD facilities. Remarkably, these results are obtained for a range of nondegenerate DM masses well below the TeV scale.

ACKNOWLEDGMENTS

M. J. R. and O. R. acknowledge the financial support given by the UdeA/CODI Grant No. 2020-33177. O. R. received further funding from MinCiencias through the Grant No. 80740-492-202. O. Z. has been partially supported by Sostenibilidad-UdeA, the UdeA/Comité para el Desarrollo de la Investigación Grants No. 2022-52380 and No. 2023-59130, and Ministerio de Ciencias Grant CD 82315 CT ICETEX 2021-1080. O. Z. would like to acknowledge support from the ICTP through the Associates Programme (2023–2028).

[1] N. Aghanim *et al.* (Planck Collaboration), Planck 2018 results. VI. Cosmological parameters, Astron. Astrophys. **641**, A6 (2020); **652**, C4(E) (2021).

[2] G. Steigman and M. S. Turner, Cosmological constraints on the properties of weakly interacting massive particles, Nucl. Phys. **B253**, 375 (1985).

[3] G. Jungman, M. Kamionkowski, and K. Griest, Supersymmetric dark matter, Phys. Rep. **267**, 195 (1996).

[4] G. Bertone, D. Hooper, and J. Silk, Particle dark matter: Evidence, candidates and constraints, Phys. Rep. **405**, 279 (2005).

[5] B. Patt and F. Wilczek, Higgs-field portal into hidden sectors, arXiv:hep-ph/0605188.

[6] G. Arcadi, A. Djouadi, and M. Raidal, Dark matter through the Higgs portal, Phys. Rep. **842**, 1 (2020).

[7] G. Arcadi, Y. Mambrini, and F. Richard, Z-portal dark matter, J. Cosmol. Astropart. Phys. 03 (2015) 018.

[8] V. Silveira and A. Zee, Scalar phantoms, Phys. Lett. **161B**, 136 (1985).

[9] J. McDonald, Gauge singlet scalars as cold dark matter, Phys. Rev. D **50**, 3637 (1994).

[10] C. Burgess, M. Pospelov, and T. ter Veldhuis, The minimal model of nonbaryonic dark matter: A singlet scalar, Nucl. Phys. **B619**, 709 (2001).

[11] Y. G. Kim and K. Y. Lee, The minimal model of fermionic dark matter, Phys. Rev. D **75**, 115012 (2007).

[12] Y. G. Kim, K. Y. Lee, and S. Shin, Singlet fermionic dark matter, J. High Energy Phys. 05 (2008) 100.

[13] S. Baek, P. Ko, and W.-I. Park, Search for the Higgs portal to a singlet fermionic dark matter at the LHC, J. High Energy Phys. 02 (2012) 047.

[14] J. R. Ellis, J. S. Hagelin, D. V. Nanopoulos, K. A. Olive, and M. Srednicki, Supersymmetric relics from the big bang, Nucl. Phys. **B238**, 453 (1984).

[15] N. G. Deshpande and E. Ma, Pattern of symmetry breaking with two Higgs doublets, Phys. Rev. D **18**, 2574 (1978).

[16] R. Barbieri, L. J. Hall, and V. S. Rychkov, Improved naturalness with a heavy Higgs: An alternative road to LHC physics, Phys. Rev. D **74**, 015007 (2006).

[17] M. Schumann, Direct detection of WIMP dark matter: Concepts and status, J. Phys. G **46**, 103003 (2019).

[18] Y. Meng *et al.* (PandaX-4T Collaboration), Dark matter search results from the PandaX-4T commissioning run, Phys. Rev. Lett. **127**, 261802 (2021).

[19] J. Aalbers *et al.* (LZ Collaboration), First dark matter search results from the LUX-ZEPLIN (LZ) experiment, Phys. Rev. Lett. **131**, 041002 (2023).

[20] E. Aprile *et al.* (XENON Collaboration), First dark matter search with nuclear recoils from the XENONnT experiment, Phys. Rev. Lett. **131**, 041003 (2023).

[21] L. Lopez Honorez, E. Nezri, J. F. Oliver, and M. H. G. Tytgat, The inert doublet model: An archetype for dark matter, J. Cosmol. Astropart. Phys. 02 (2007) 028.

[22] C. Boehm, P. Fayet, and J. Silk, Light and heavy dark matter particles, Phys. Rev. D **69**, 101302 (2004).

[23] E. Ma, Supersymmetric model of radiative seesaw Majorana neutrino masses, Ann. Fond. Louis Broglie **31**, 285 (2006).

[24] Q.-H. Cao, E. Ma, J. Wudka, and C. P. Yuan, Multipartite dark matter, arXiv:0711.3881.

[25] T. Hur, H.-S. Lee, and S. Nasri, A supersymmetric U(1)-prime model with multiple dark matters, Phys. Rev. D **77**, 015008 (2008).

[26] H.-S. Lee, Lightest U-parity particle (LUP) dark matter, Phys. Lett. B **663**, 255 (2008).

[27] K. M. Zurek, Multi-component dark matter, Phys. Rev. D **79**, 115002 (2009).

[28] V. Barger, P. Langacker, M. McCaskey, M. Ramsey-Musolf, and G. Shaughnessy, Complex singlet extension of the standard model, Phys. Rev. D **79**, 015018 (2009).

[29] S. Profumo, K. Sigurdson, and L. Ubaldi, Can we discover multi-component WIMP dark matter?, J. Cosmol. Astropart. Phys. 12 (2009) 016.

[30] T. Hambye, Hidden vector dark matter, J. High Energy Phys. 01 (2009) 028.

[31] F. D'Eramo and J. Thaler, Semi-annihilation of dark matter, J. High Energy Phys. 06 (2010) 109.

[32] N. Bernal, D. Restrepo, C. Yaguna, and O. Zapata, Two-component dark matter and a massless neutrino in a new $B-L$ model, Phys. Rev. D **99**, 015038 (2019).

[33] A. Poulin and S. Godfrey, Multicomponent dark matter from a hidden gauged SU(3). Phys. Rev. D **99**, 076008 (2019).

[34] D. Borah, R. Roshan, and A. Sil, Minimal two-component scalar doublet dark matter with radiative neutrino mass, Phys. Rev. D **100**, 055027 (2019).

[35] D. Nanda and D. Borah, Connecting light Dirac neutrinos to a multi-component dark matter scenario in gauged $B-L$ model, Eur. Phys. J. C **80**, 557 (2020).

[36] S. Bhattacharya, P. Ghosh, and N. Sahu, Multipartite dark matter with scalars, fermions and signatures at LHC, J. High Energy Phys. 02 (2019) 059.

[37] S. Bhattacharya, P. Ghosh, A. K. Saha, and A. Sil, Two component dark matter with inert Higgs doublet: Neutrino mass, high scale validity and collider searches, J. High Energy Phys. 03 (2020) 090.

[38] A. Betancur, G. Palacio, and A. Rivera, Inert doublet as multicomponent dark matter, Nucl. Phys. **B962**, 115276 (2021).

[39] J. Hernandez-Sanchez, V. Keus, S. Moretti, D. Rojas-Ciofalo, and D. Sokolowska, Complementary probes of two-component dark matter, arXiv:2012.11621.

[40] G. Bélanger, A. Pukhov, C. E. Yaguna, and O. Zapata, The Z_5 model of two-component dark matter, J. High Energy Phys. 09 (2020) 030.

[41] S.-M. Choi, J. Kim, P. Ko, and J. Li, A multi-component SIMP model with $U(1)_X \to Z_2 \times Z_3$, J. High Energy Phys. 09 (2021) 028.

[42] G. Belanger, A. Mjallal, and A. Pukhov, Two dark matter candidates: The case of inert doublet and singlet scalars, Phys. Rev. D **105**, 035018 (2022).

[43] B. Díaz Sáez, P. Escalona, S. Norero, and A. R. Zerwekh, Fermion singlet dark matter in a pseudoscalar dark matter portal, J. High Energy Phys. 10 (2021) 233.

[44] A. Mohamadnejad, Electroweak phase transition and gravitational waves in a two-component dark matter model, J. High Energy Phys. 03 (2022) 188.

[45] N. Chakrabarty, R. Roshan, and A. Sil, Two-component doublet-triplet scalar dark matter stabilizing the electroweak vacuum, Phys. Rev. D **105**, 115010 (2022).

[46] S.-Y. Ho, P. Ko, and C.-T. Lu, Scalar and fermion two-component SIMP dark matter with an accidental $\mathbb{Z}_4$ symmetry, J. High Energy Phys. 03 (2022) 005.
[47] S. Bhattacharya, P. Ghosh, J. Lahiri, and B. Mukhopadhyaya, Distinguishing two dark matter component particles at e^+e^- colliders, J. High Energy Phys. 12 (2022) 049.
[48] A. Dutta Banik, R. Roshan, and A. Sil, Two component singlet-triplet scalar dark matter and electroweak vacuum stability, Phys. Rev. D **103**, 075001 (2021).
[49] J. Hernandez-Sanchez, V. Keus, S. Moretti, and D. Sokolowska, Complementary collider and astrophysical probes of multi-component dark matter, J. High Energy Phys. 03 (2023) 045.
[50] A. Bas i Beneito, J. Herrero-García, and D. Vatsyayan, Multi-component dark sectors: Symmetries, asymmetries and conversions, J. High Energy Phys. 10 (2022) 075.
[51] E. Hall, T. Konstandin, R. McGehee, and H. Murayama, Asymmetric matter from a dark first-order phase transition, Phys. Rev. D **107**, 055011 (2023).
[52] E. Hall, R. McGehee, H. Murayama, and B. Suter, Asymmetric dark matter may not be light, Phys. Rev. D **106**, 075008 (2022).
[53] C. E. Yaguna and O. Zapata, Two-component scalar dark matter in Z_{2n} scenarios, J. High Energy Phys. 10 (2021) 185.
[54] C. E. Yaguna and O. Zapata, Fermion and scalar two-component dark matter from a Z4 symmetry, Phys. Rev. D **105**, 095026 (2022).
[55] A. Das, S. Gola, S. Mandal, and N. Sinha, Two-component scalar and fermionic dark matter candidates in a generic U(1)X model, Phys. Lett. B **829**, 137117 (2022).
[56] G. Bélanger, A. Pukhov, C. E. Yaguna, and O. Zapata, The Z_7 model of three-component scalar dark matter, J. High Energy Phys. 03 (2023) 100.
[57] M. Hosseini, S. Yaser Ayazi, and A. Mohamadnejad, Gravitational wave effects and phenomenology of a two-component dark matter model, Eur. Phys. J. C **84**, 485 (2024).
[58] C. E. Yaguna and O. Zapata, Minimal model of fermion FIMP dark matter, Phys. Rev. D **109**, 015002 (2024).
[59] C. E. Yaguna and O. Zapata, Multi-component scalar dark matter from a Z_N symmetry: A systematic analysis, J. High Energy Phys. 03 (2020) 109.
[60] P. Van Dong, C. H. Nam, and D. Van Loi, Canonical seesaw implication for two-component dark matter, Phys. Rev. D **103**, 095016 (2021).
[61] C. E. Yaguna and O. Zapata, Singlet Dirac dark matter streamlined, J. Cosmol. Astropart. Phys. 06 (2024) 049.
[62] M. L. Graesser, I. M. Shoemaker, and L. Vecchi, Asymmetric WIMP dark matter, J. High Energy Phys. 10 (2011) 110.
[63] A. Bas i Beneito, J. Herrero-García, and D. Vatsyayan, Multi-component dark sectors: Symmetries, asymmetries and conversions, J. High Energy Phys. 10 (2022) 075.
[64] J. Herrero-Garcia, G. Landini, and D. Vatsyayan, Asymmetries in extended dark sectors: A cogenesis scenario, J. High Energy Phys. 05 (2023) 049.
[65] G. Aad *et al.* (ATLAS, CMS Collaborations), Combined measurement of the Higgs boson mass in pp collisions at $\sqrt{s} = 7$ and 8 TeV with the ATLAS and CMS experiments, Phys. Rev. Lett. **114**, 191803 (2015).
[66] H. Beauchesne and C.-W. Chiang, Dark matter semi-annihilation for inert scalar multiplets, J. High Energy Phys. 06 (2024) 164.
[67] G. Bélanger, F. Boudjema, A. Pukhov, and A. Semenov, micrOMEGAs4.1: Two dark matter candidates, Comput. Phys. Commun. **192**, 322 (2015).
[68] G. Alguero, G. Belanger, F. Boudjema, S. Chakraborti, A. Goudelis, S. Kraml, A. Mjallal, and A. Pukhov, micrOMEGAs 6.0: N-component dark matter, Comput. Phys. Commun. **299**, 109133 (2024).
[69] A. Semenov, LanHEP—A package for automatic generation of Feynman rules from the Lagrangian. Version 3.2, Comput. Phys. Commun. **201**, 167 (2016).
[70] J. Hisano, R. Nagai, and N. Nagata, Singlet Dirac Fermion dark matter with mediators at loop, J. High Energy Phys. 12 (2018) 059.
[71] E. Aprile *et al.* (XENON100 Collaboration), Likelihood approach to the first dark matter results from XENON100, Phys. Rev. D **84**, 052003 (2011).
[72] J. Herrero-Garcia, A. Scaffidi, M. White, and A. G. Williams, On the direct detection of multi-component dark matter: Sensitivity studies and parameter estimation, J. Cosmol. Astropart. Phys. 11 (2017) 021.
[73] J. Herrero-Garcia, A. Scaffidi, M. White, and A. G. Williams, On the direct detection of multi-component dark matter: Implications of the relic abundance, J. Cosmol. Astropart. Phys. 01 (2019) 008.
[74] R. H. Helm, Inelastic and elastic scattering of 187-Mev electrons from selected even-even nuclei, Phys. Rev. **104**, 1466 (1956).
[75] J. Lewin and P. Smith, Review of mathematics, numerical factors, and corrections for dark matter experiments based on elastic nuclear recoil, Astropart. Phys. **6**, 87 (1996).
[76] A. K. Drukier, K. Freese, and D. N. Spergel, Detecting cold dark-matter candidates, Phys. Rev. D **33**, 3495 (1986).
[77] K. Freese, J. Frieman, and A. Gould, Signal modulation in cold-dark-matter detection, Phys. Rev. D **37**, 3388 (1988).
[78] E. Aprile *et al.* (XENON Collaboration), Dark matter search results from a one ton-year exposure of XENON1T, Phys. Rev. Lett. **121**, 111302 (2018).
[79] R. N. Lerner and J. McDonald, Gauge singlet scalar as inflaton and thermal relic dark matter, Phys. Rev. D **80**, 123507 (2009).
[80] M. D. Goodsell and F. Staub, Unitarity constraints on general scalar couplings with SARAH, Eur. Phys. J. C **78**, 649 (2018).
[81] G. Bélanger, K. Kannike, A. Pukhov, and M. Raidal, Minimal semi-annihilating $\mathbb{Z}_N$ scalar dark matter, J. Cosmol. Astropart. Phys. 06 (2014) 021.
[82] I. F. Ginzburg and M. Krawczyk, Symmetries of two Higgs doublet model and CP violation, Phys. Rev. D **72**, 115013 (2005).
[83] K. Kannike, Vacuum stability conditions from copositivity criteria, Eur. Phys. J. C **72**, 2093 (2012).
[84] F. Staub, SARAH 4: A tool for (not only SUSY) model builders, Comput. Phys. Commun. **185**, 1773 (2014).
[85] F. Staub, Exploring new models in all detail with SARAH, Adv. High Energy Phys. **2015**, 840780 (2015).

[86] M. E. Peskin and T. Takeuchi, Estimation of oblique electroweak corrections, Phys. Rev. D **46**, 381 (1992).
[87] M. Baak, J. Cúth, J. Haller, A. Hoecker, R. Kogler, K. Mönig, M. Schott, and J. Stelzer (Gfitter Group), The global electroweak fit at NNLO and prospects for the LHC and ILC, Eur. Phys. J. C **74**, 3046 (2014).
[88] P. Posch, Enhancement of $h \to \gamma\gamma$ gamma in the two Higgs doublet model type I, Phys. Lett. B **696**, 447 (2011).
[89] ATLAS Collaboration, Measurements and interpretations of Higgs-boson fiducial cross sections in the diphoton decay channel using 139 fb^{-1} of pp collision data at $\sqrt{s} =$ 13 TeV with the ATLAS detector, J. High Energy Phys. 08 (2022) 027.
[90] A. M. Sirunyan *et al.* (CMS Collaboration), Measurements of Higgs boson production cross sections and couplings in the diphoton decay channel at $\sqrt{s} = 13$ TeV, J. High Energy Phys. 07 (2021) 027.
[91] T. Abe, R. Kitano, and R. Sato, Discrimination of dark matter models in future experiments, Phys. Rev. D **91**, 095004 (2015); **96**, 019902(E) (2017).
[92] A. M. Sirunyan *et al.* (CMS Collaboration), Search for invisible decays of a Higgs boson produced through vector boson fusion in proton-proton collisions at $\sqrt{s} = 13$ TeV, Phys. Lett. B **793**, 520 (2019).
[93] ATLAS Collaboration, Search for invisible Higgs boson decays with vector boson fusion signatures with the ATLAS detector using an integrated luminosity of 139 fb^{-1}, J. High Energy Phys. 08 (2022) 104.
[94] P. A. Zyla *et al.* (Particle Data Group), Review of particle physics, Prog. Theor. Exp. Phys. **2020**, 083C01 (2020).
[95] A. Pierce and J. Thaler, Natural dark matter from an unnatural Higgs boson and new colored particles at the TeV scale, J. High Energy Phys. 08 (2007) 026.
[96] L. Baudis, A. Behrens, A. Ferella, A. Kish, T. Marrodan Undagoitia, D. Mayani, and M. Schumann, Performance of the Hamamatsu R11410 photomultiplier tube in cryogenic Xenon environments, J. Instrum. **8**, P04026 (2013).
[97] D. S. Akerib *et al.* (LZ Collaboration), Projected WIMP sensitivity of the LUX-ZEPLIN dark matter experiment, Phys. Rev. D **101**, 052002 (2020).
[98] M. Cirelli, E. Del Nobile, and P. Panci, Tools for model-independent bounds in direct dark matter searches, J. Cosmol. Astropart. Phys. 10 (2013) 019.
[99] E. Aprile *et al.* (XENON Collaboration), Dark matter search results from a one ton-year exposure of XENON1T, Phys. Rev. Lett. **121**, 111302 (2018).
[100] B. J. Mount *et al.*, LUX-ZEPLIN (LZ) technical design report, arXiv:1703.09144.
[101] S. Yellin, Finding an upper limit in the presence of an unknown background, Phys. Rev. D **66**, 032005 (2002).
[102] M. Cirelli, N. Fornengo, and A. Strumia, Minimal dark matter, Nucl. Phys. **B753**, 178 (2006).
[103] T. Hambye, F. S. Ling, L. Lopez Honorez, and J. Rocher, Scalar multiplet dark matter, J. High Energy Phys. 07 (2009) 090; 05 (2010) 066(E).
[104] M. Cirelli, A. Strumia, and M. Tamburini, Cosmology and astrophysics of minimal dark matter, Nucl. Phys. **B787**, 152 (2007).